Chaos
An Interdisciplinary Journal of Nonlinear Science

RESEARCH ARTICLE | SEPTEMBER 19 2025

Collapse of multi-headed chimera states in biologically based neuronal networks

Lucas E. Bentivoglio ; Diogo L. M. Souza ; Enrique C. Gabrick ; Paulo R. Protachevicz ; Gustavo A. Sousa ; Iberê L. Caldas ; Ricardo L. Viana ; Kelly C. Iarosz ; Antonio M. Batista ; Fernando S. Borges

Check for updates

Chaos 35, 093144 (2025)
https://doi.org/10.1063/5.0282696

View Online
Export Citation

Articles You May Be Interested In

Chimera states in a multilayer network of coupled and uncoupled neurons
Chaos (July 2017)

Mixed-mode chimera states in pendula networks
Chaos (October 2022)

Identification of chimera using machine learning
Chaos (June 2020)

22 September 2025 13:44:29

Chaos
Special Topics Open for Submissions
Learn More
AIP Publishing

AIP Publishing

Collapse of multi-headed chimera states in biologically based neuronal networks

Cite as: Chaos 35, 093144 (2025); doi: 10.1063/5.0282696
Submitted: 27 May 2025 · Accepted: 7 September 2025 ·
Published Online: 19 September 2025

View Online Export Citation CrossMark

Lucas E. Bentivoglio,[1,a)] Diogo L. M. Souza,[1] Enrique C. Gabrick,[2] Paulo R. Protachevicz,[3] Gustavo A. Sousa,[1] Iberê L. Caldas,[2] Ricardo L. Viana,[4] Kelly C. Iarosz,[5] Antonio M. Batista,[1,6] and Fernando S. Borges[1,7,8]

AFFILIATIONS

[1]Graduate Program in Science, State University of Ponta Grossa, 84030-900 Ponta Grossa, PR, Brazil
[2]Institute of Physics, University of São Paulo, 05508-090 São Paulo, SP, Brazil
[3]Graduate Program in Electrical Engineering and Industrial Informatics, Federal University of Technology—Paraná, 80230-901 Curitiba, PR, Brazil
[4]Department of Physics and Interdisciplinary Centre of Science, Technology, and Innovation, NMCC, Federal University of Paraná, 81531-980 Curitiba, PR, Brazil
[5]University Center UNIFATEB, 84266-010 Telêmaco Borba, PR, Brazil
[6]Department of Mathematics and Statistics, State University of Ponta Grossa, 84030-900 Ponta Grossa, PR, Brazil
[7]Department of Physiology and Pharmacology, State University of New York Downstate Health Sciences University, Brooklyn, New York 11203, USA
[8]Center for Mathematics, Computation, and Cognition, Federal University of ABC, 09606045 São Bernardo do Campo, SP, Brazil

[a)]**Author to whom correspondence should be addressed:** lucas16edu@gmail.com

ABSTRACT

Chimera states are spatiotemporal patterns with coherent and incoherent dynamics coexisting. These patterns are believed to be involved in important neurophysiological phenomena, such as unihemispheric sleep, multitasking, and epileptic seizures. We explore the emergence and collapse of chimeras in a network of locally coupled excitatory neurons. We consider a biologically realistic conductance-based neuron model that incorporates slow potassium and calcium ion channels, enabling the reproduction of pyramidal neuron dynamics. By varying the coupling strength and the local connectivity radius, we identify transitions from regular spiking to chimera states with one or more incoherent domains. We demonstrate that the number of heads depends on the neuronal connectivity. The multi-headed chimeras exhibit shorter average collapse times than single-headed ones. Our findings contribute to a deeper understanding of transient spatiotemporal structures in biologically inspired excitable models.

Published under an exclusive license by AIP Publishing. https://doi.org/10.1063/5.0282696

In the study of brain dynamics, researchers have identified dynamic patterns in which some groups of neurons exhibit synchronized activities while others remain desynchronized, known as chimera states. Chimeras have been associated with neurophysiological phenomena, such as unihemispheric sleep, attention, and epileptic seizures. In this work, we investigate the formation and collapse of chimera states in a network composed of conductance-based neurons. The neuron model includes sodium, potassium, and calcium ion channels, allowing us to reproduce the electrophysiological behavior of cortical pyramidal neurons. We explore how the spatial arrangement and strength of excitatory synaptic connections influence the emergence of chimera states. We focus on patterns that contain multiple desynchronized regions, with each region corresponding to a head. We show that chimera states with a greater number of heads tend to collapse more quickly than those with a single head. Furthermore, we demonstrate that small variations in the initial conditions can affect the chimera lifespans. Our results offer valuable insights into how brain connectivity and synaptic interactions can contribute to healthy brain functions and the development of neurological disorders.

22 September 2025 13:44:29

I. INTRODUCTION

Networked dynamical systems exhibit a rich variety of spatiotemporal patterns.[1] Depending on the coupling strength and the number of connections, the systems can exhibit synchronization, chaos, or partial coherence.[2,3] In coupled oscillator networks, synchronization emerges from mutual adjustment of individual rhythms[4] and has been extensively studied in classical models, such as phase oscillators. Over the years, many studies have been conducted on the synchronization patterns of phase oscillators.[5,6]

A particularly interesting phenomenon is the chimera state, a spatiotemporal pattern where coherent and incoherent dynamics coexist despite symmetry and homogeneous coupling.[7–10] Chimeras were first identified in arrays of phase oscillators.[11] They have been reported in a wide range of systems, including chemical oscillators,[12,13] spatial light modulators,[14] and natural populations, such as fireflies.[15] These patterns have also been found in neuronal systems.[16–18]

In neuroscience, chimera states have gained attention for their potential role in brain dynamics. Biological analogs include unihemispheric sleep in dolphins and birds, where one hemisphere remains active while the other sleeps.[19,20] Asymmetries have also been observed in EEG recordings during motor coordination tasks.[21] Chimera patterns have been related to pathological transitions, such as epileptic seizures and Parkinsonian synchronization.[22–24]

A key tool for assessing the effects and understanding the mechanism of chimera states in neural networks are represented through mathematical models. Significant results have been obtained using coupled neuron models, e.g., integrate-and-fire,[25] Morris–Lecar,[26] FitzHugh–Nagumo,[27] Hindmarsh–Rose,[28] and Hodgkin–Huxley[29] neurons. In particular, Santos *et al.*[30] showed chimera states in a connectivity matrix based on the cat brain with coupled Hindmarsh–Rose neurons. They employ recurrence analysis to detect spike and burst chimeras. Despite these advances, the mechanisms behind the emergence and collapse of chimeras in biologically accurate neuronal models remain not fully understood.

In this work, we explore the dynamics of a locally connected network of excitatory pyramidal neurons. The pyramidal neurons are characterized by their pyramidal shape of the soma. They are the most populous members of the excitatory family in the brain, receiving and transmitting information as well as increasing the probability that connected neurons fire. These neurons are found in various regions of the central nervous system, for instance, hippocampus and cerebral cortex. Each neuron is modeled using a conductance-based model that includes slow potassium as well as high- and low-threshold calcium currents, capturing important physiological features of cortical excitatory cells.[31–33] We systematically vary the number of nearest neighbors and the coupling strength to identify synchronous and asynchronous spikes, bursts, and chimera states. Additionally, we also investigate how initial conditions influence the collapse time of chimera states, defined as the moment when incoherent domains disappear. We find that the collapse is highly sensitive to the initial conditions, with multi-headed chimeras collapsing faster than single-headed ones. Our results suggest that abrupt transitions in the dynamic behavior of the neurons, reminiscent of seizure onset, can be triggered by subtle variations in the network state.

One of our main contributions is to build a network model composed of biologically realistic conductance-based neurons connected to the nearest neighbors. The novelty in our network is the emergence of multi-headed chimera states. Our findings contribute to a deeper understanding of spatiotemporal pattern formation in excitable systems and can offer insights into the dynamics of neurological phenomena.

This article is organized as follows: Section II presents the neuron model and the neuronal network, including descriptions of the ionic currents and synaptic coupling. We also introduced the diagnostic tools to characterize the network dynamics. In Sec. III, we report our main results, discussing the emergence of chimera states, their collapse dynamics, and how the collapse times vary under different initial conditions. Finally, in Sec. IV, we summarize our conclusions and highlight the implications of our findings.

II. NEURONAL NETWORK

To describe each neuron i in the network, we consider a conductance-based model[32] in which the membrane potential is given by

$$C_m \frac{dV}{dt} = -g_{\text{leak}}(V - E_{\text{leak}}) - I_{\text{ionic}}, \tag{1}$$

where $C_m = 1\ \mu\text{F/cm}^2$ is the membrane capacitance, g_{leak} is the leak conductance, E_{leak} is the reversal potential, and I_{ionic} is the sum of the ionic currents I_j.

All the ionic currents are voltage-dependent and can be described by the general equation

$$I_j = g_j m^l h^p (V - E_j), \tag{2}$$

where the jth ionic current I_j is expressed as the product of the maximum conductance for each ion j with conductance g_j. The variables m and h are related to the ionic channel activation and inactivation, respectively, with order l and p.[34] The difference between E_j and V is the reversal potential for a specific ion.[32]

In addition to the classic currents of sodium (I_{Na}) and potassium (I_K) from the Hodgkin–Huxley model, we add the currents of slow potassium (I_M),[35] high-threshold calcium (I_L),[36] and low-threshold calcium (I_T).[37] To include these ionic currents in the model, we define the term I^i_{ionic} as the sum of the ionic currents, which is given by

$$I^i_{\text{ionic}} = I_{Na} + I_k + I_M + I_L + I_T. \tag{3}$$

In the classical Hodgkin–Huxley model, the voltage-dependent potassium and sodium currents were described for a squid axon. Afterward, Traub and Miles[38] adapted the equations for central neurons. They obtained a potassium current that is described by the following set of equations:

$$\begin{aligned} I_K &= g_K n^4 (V - E_K), \\ \frac{dn}{dt} &= \alpha_n(V)(1 - n) - \beta_n(V) n, \\ \alpha_n &= \frac{-0.32(V - V_T - 15)}{\exp[-(V - V_T - 15)/5] - 1}, \\ \beta_n &= 0.5 \exp[-(V - V_T - 10)/40], \end{aligned} \tag{4}$$

22 September 2025 13:44:29

Published under an exclusive license by AIP Publishing

and the sodium currents are described by

$$
\begin{aligned}
I_{Na} &= g_{Na} m^3 h (V - E_{Na}),\\
\frac{dm}{dt} &= \alpha_m(V)(1-m) - \beta_m(V) m,\\
\frac{dh}{dt} &= \alpha_h(V)(1-h) - \beta_h(V) h,\\
\alpha_m &= \frac{-0.32(V - V_T - 13)}{\exp[-(V - V_T - 40)/5] - 1},\\
\beta_m &= \frac{0.28(V - V_T - 40)}{\exp[(V - V_T - 40)/5] - 1},\\
\alpha_h &= 0.128 \exp[-(V - V_T - 17)/18],\\
\beta_h &= \frac{4}{1 + \exp[-(V - V_T - 40)/5]}.
\end{aligned}
\tag{5}
$$

The conductances of potassium and sodium are $g_K = 5\,\mathrm{mS/cm^2}$ and $g_{Na} = 50\,\mathrm{mS/cm^2}$, respectively, and the reversal potentials are $E_k = -100\,\mathrm{mV}$ and $E_{Na} = 50\,\mathrm{mV}$. In our simulations, we consider $V_T = -55\,\mathrm{mV}$. The I_M current is related to the slow potassium current due to the fact that it operates on a slower timescale than the potassium current. This current acts as a frequency adapter in neuronal activity.[39] In other words, the I_M current functions as an inhibitor of neuronal spiking and is given by

$$
I_M = g_M p (V - E_K), \tag{6}
$$

where

$$
\begin{aligned}
\frac{dp}{dt} &= (p_\infty(V) - p)/\tau_p(V),\\
p_\infty(V) &= \frac{1}{1 + \exp[-(v + 35)/10]},\\
\tau_p(V) &= \frac{\tau_{\max}}{3.3 \exp[(V + 35)/20] + \exp[-(V + 35)/20]},
\end{aligned}
\tag{7}
$$

with $g_M = 0.03\,\mathrm{mS/cm^2}$ and $\tau_{\max} = 1000\,\mathrm{ms}$.[35,40]

Although in smaller quantities compared to other ions, the currents I_L and I_T play an important role in the neuronal activities. Their presence is required for generation of bursting activities. The set of equations that describes I_L current is given by

$$
\begin{aligned}
I_L &= g_L q^2 r (V - E_{Ca}),\\
\frac{dq}{dt} &= \alpha_q(V)(1-q) - \beta_q(V) q,\\
\frac{dr}{dt} &= \alpha_r(V)(1-r) \beta_r(V) r,\\
\alpha_q &= \frac{0.055(-27 - V)}{\exp[(-27 - V)/3.8] - 1},\\
\beta_q &= 0.94 \exp[(-75 - b)/17],\\
\alpha_r &= 0.000\,457 \exp[(-13 - V)/50],\\
\beta_r &= \frac{0.0065}{\exp[(-15 - V)/28] + 1},
\end{aligned}
\tag{8}
$$

where $g_L = 0.3\,\mathrm{mS/cm^2}$ is the maximum value of conductance and $E_{Ca} = 120\,\mathrm{mV}$[36] is the reversal potential of the calcium. The I_T current is described by

$$
\begin{aligned}
I_T &= g_T s_\infty^2 u (V - E_{Ca}),\\
\frac{du}{dt} &= (u_\infty(V) - u)/\tau_u(V),\\
s_\infty(V) &= \frac{1}{1 + \exp[-(V + V_x + 57)/62]},\\
u_\infty(V) &= \frac{1}{1 + \exp[-(V + V_x + 81)/4]},\\
\tau_u(V) &= 30.8 + \frac{211.4 + \exp[(V + V_x + 113.2)/5]}{1 + \exp[(V + V_x + 84)/3.2]},
\end{aligned}
$$

where $g_T = 1\,\mathrm{mS/cm^2}$ is the maximum conductance of the I_T current and $V_x = 2\,\mathrm{mV}$.[37,41] The functions $s_\infty(V)$ and $u_\infty(V)$ are related to the opening and closing of the ion channel. The function $\tau_u(V)$ indicates how long the ion channel remains open.

We construct a local network in which each neuron [Eq. (1)] is connected to the R nearest neighbors. Therefore, a neuron i is connected with every neuron j within a range of R, i.e., $|i - j| <= R$ for $i, j = 1, 2, 3, \ldots, N$. Throughout this work, we fix the network size to $N = 1000$ excitatory neurons. We consider closed boundary conditions, so all neurons send and receive $2R$ connections. Synaptic coupling is incorporated by adding the synaptic current term I_{syn} to Eq. (1) as follows:

$$
C_m \frac{dV_i}{dt} = -g_{\mathrm{leak}}(V_i - E_{\mathrm{leak}}) - I^i_{\mathrm{ionic}} + I^i_{\mathrm{syn}} + I/A, \tag{9}
$$

where $C_m = 1\,\mu\mathrm{F/cm^2}$ is the specific capacitance of the membrane and $A = 0.2835 \times 10^{-3}\,\mathrm{cm^2}$ is the membrane area.[40] V_i is the membrane potential, g_{leak} is the leak membrane conductance, E_{leak} is the resting potential, and I is a constant current that is equal to all neurons (μA). The synaptic current I^i_{syn} is given by

$$
I^i_{\mathrm{syn}} = \sum_{k=1}^{N} \left(V^k_{\mathrm{rev}} - V_i\right) M_{ik} g_{\mathrm{syn}}, \tag{10}
$$

where $V^{\mathrm{k}}_{\mathrm{rev}} = 0$ represents the excitatory synaptic reversal potential, g_{syn} is the synaptic conductance from the neuron k, and M_{ik} is the adjacent matrix of connections; when $M_{ik} = 1$ (0), the k neuron is connected (or non-connected) with an i-neuron. Observe that $M_{ik} = 0$ for all $i = k$, i.e., no self-connections.

III. DIAGNOSTIC TOOLS

The coefficient of variation (CV) is commonly used to differentiate spikes and bursts. To calculate the CV, we define the interspike interval (ISI) as the time interval between two consecutive neuronal spikes, $t_{i,m+1}$ and $t_{i,m}$; thus, $\mathrm{ISI}_i = t_{i,m+1} - t_{i,m}$. The ratio between the standard deviation and the mean ISI (indicated by $\langle \mathrm{ISI}_i \rangle$) gives rise to CV_i,

$$
\mathrm{CV}_i = \frac{\sqrt{\left\langle (\mathrm{ISI}_i - \langle \mathrm{ISI}_i \rangle)^2 \right\rangle}}{\langle \mathrm{ISI}_i \rangle}. \tag{11}
$$

22 September 2025 13:44:29

Published under an exclusive license by AIP Publishing

The average CV for the entire network is defined as

$$\mathrm{CV} = \frac{1}{N}\sum_{i=1}^{N} \mathrm{CV}_i; \tag{12}$$

when CV < 0.5, the neurons are in the spike regime, while CV ≥ 0.5 defines the emergence of burst activities.

The desynchronous and synchronous patterns can be identified using the local and global phase order parameter.[42] Each neuron is defined a local phase order parameter by computing the phase of the five neighbors on the right and on the left (totaling 10 connections),

$$Z_j(t) = \left| \frac{1}{10+1} \sum_{|j-i|\leqslant 5} \exp(i\phi_i(t)) \right|, i = 1, \ldots, N; \tag{13}$$

the phase is defined as

$$\phi_i(t) = 2\pi \left(m + \frac{t - t_{i,m}}{t_{i,m+1} - t_{i,m}} \right), \tag{14}$$

where $t_{i,m}$ is the time of the mth spike of the neuron i, with $t_{i,m} < t < t_{i,m+1}$. In our simulations, we consider that the patterns are locally synchronized if $Z_j > 0.9$, computing in the last 10 ms.

Unlike the local order parameter, the global order parameter (Z_g) measures the synchronization degree of the whole network, and it is defined as

$$Z_g(t) = \frac{1}{N}\sum_{j=1}^{N} Z_j(t), \tag{15}$$

where $N = 1000$ is the number of neurons in the network. The temporal mean value of Z_g for the time window $t_{\mathrm{fin}} - t_{\mathrm{ini}}$ is

$$\equiv \frac{1}{t_{\mathrm{fin}} - t_{\mathrm{ini}}} \int_{t_{\mathrm{ini}}}^{t_{\mathrm{fin}}} Z_(g(t))\, dt. \tag{16}$$

IV. CHIMERA HEADS AND COLLAPSE TIME

We investigate the transitions between the firing patterns by varying R and g_{syn} (Fig. 1). To do that, we compute the values of CV and $\overline{Z}_g$, as shown in panels (a) and (b), respectively. For low coupling strength $g_{\mathrm{syn}} < 0.1\,\mathrm{mS/cm^2}$ and $R < 5$, highlighted by the cyan square in Fig. 1(a), the neurons exhibit desynchronous activities with irregular spike patterns [Fig. 1(c)]. Increasing g_{syn} and R, the neurons exhibit a spike regime with regular behavior, as displayed in Fig. 1(d). Consequently, CV < 0.5 and $\overline{Z}_g$ increases. For CV equal to 0.03, it is possible to observe the coexistence of desynchronous and synchronous dynamics, known as a chimera state [Fig. 1(e)].[43] The domains with desynchronized neurons are called heads. For large values of R and g_{syn}, the neurons exhibit bursting activities, as shown in Fig. 1(f). In the white red region, the averaged firing frequency exceeds 40 Hz. Since these values exceed the typical physiological range observed in cortical pyramidal neurons, we consider this threshold as an upper limit.

To identify and track chimera states, we compute the local phase order parameter Z_j over a time window of $\tau = 300$ ms. We consider that there is a chimera state when five or more consecutive

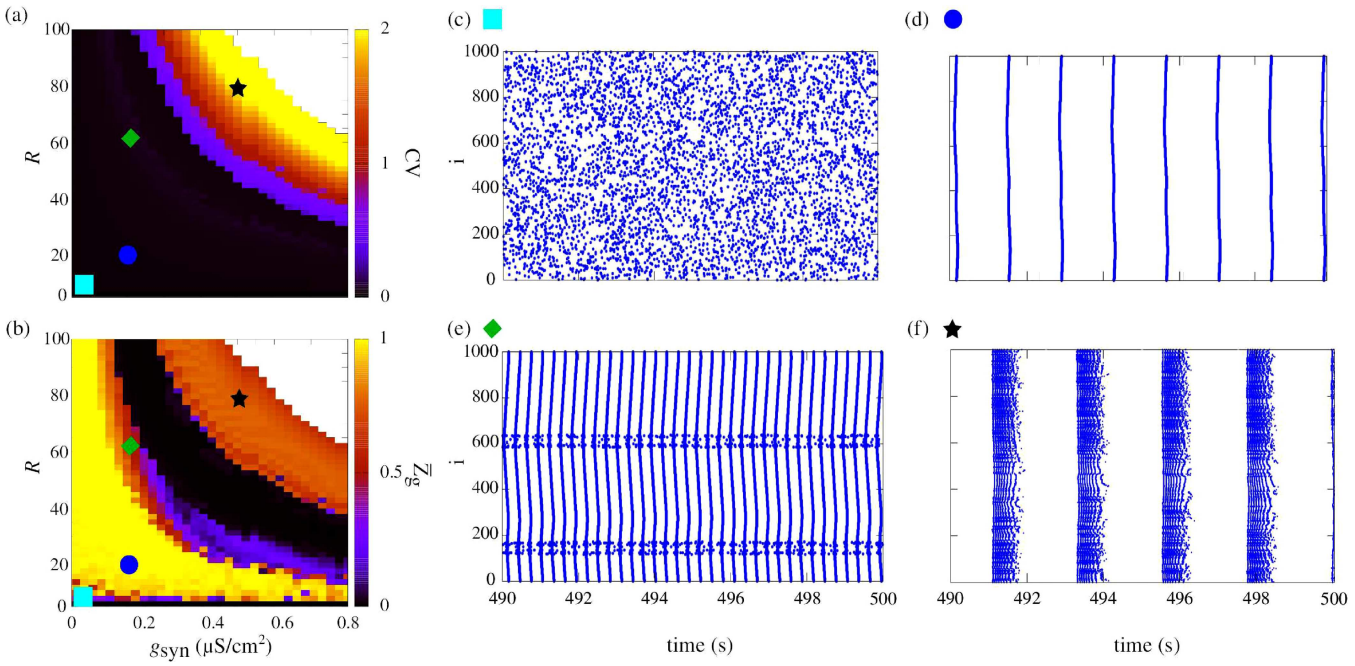


FIG. 1. Firing pattern for different R and g_{syn}, where the color bars denote the values of (a) CV and (b) $\overline{Z}_g$. Raster plots for (c) $R = 5$ and $g_{\mathrm{syn}} = 0.06\,\mathrm{mS/cm^2}$, (d) $R = 20$ and $g_{\mathrm{syn}} = 0.2\,\mathrm{mS/cm^2}$, (e) $R = 50$ and $g_{\mathrm{syn}} = 0.25\,\mathrm{mS/cm^2}$, and (f) $R = 80$ and $g_{\mathrm{syn}} = 0.5\,\mathrm{mS/cm^2}$.

22 September 2025 13:44:29

Published under an exclusive license by AIP Publishing

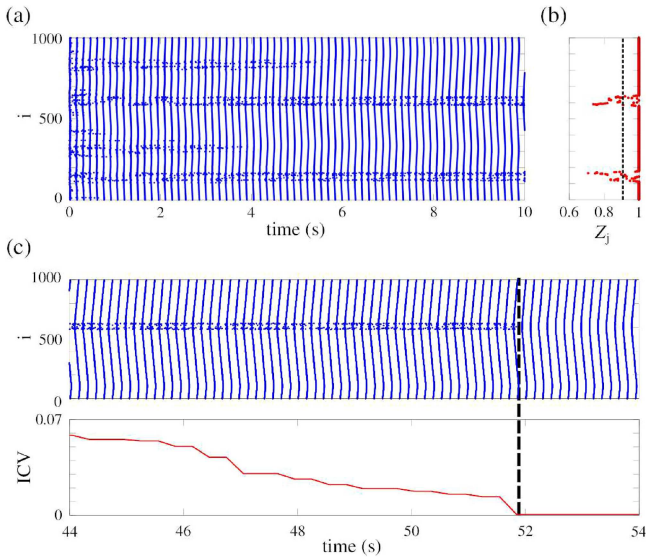


FIG. 2. (a) Raster plot for $R = 45$ and $g_{syn} = 0.3\,mS/cm^2$. Multiple chimera heads initially emerge and two heads persist. (b) Local phase order parameter Z_j for the time equal to 10 s, where the black dotted line corresponds to $Z_j = 0.9$. (c) Raster plot and temporal evolution of ICV. The black dashed line indicates the CT value (iCV< 0.01).

neurons satisfy $Z_j < 0.9$. The chimeras can emerge and vanish over time, and then the number of detected heads depends on the time window. To analyze the collapse of chimera states, we compute the instantaneous coefficient of variation (ICV). The ICV value is calculated for each neuron by means of Eq. (12). The collapse time (CT) is identified when all values of ICV is less than 0.01.

Figure 2 shows the formation and disappearance of chimera heads. Panel (a) displays a raster plot of the neuronal activities during the first 10 s of 100 s simulation. Various desynchronized regions emerge, indicating the presence of multi-headed chimera states. Many of these desynchronized domains collapse before 7 s, and two heads remain. Panel (b) exhibits the respective values of Z_j, revealing the spatial structure. In panel (c), we compute the raster plot for the time greater than 44 s and the temporal evolution of ICV. The neurons with desynchronous activities transition to a synchronous behavior. The vertical dashed line marks the CT value at which all domains with desynchronized neurons vanish and ICV < 0.01.

Concerning the chimera heads, we analyze how the number of chimera heads and their CT evolve as a function of time. Figure 3 displays the parameter spaces $g_{syn} \times R$ for (a) 25, (b) 100, and (c) 500 s. The top panels show the number of chimera heads identified at the final time, while the bottom panels display the respective CT of the chimera heads. For 25 s, Fig. 3(a) exhibits the presence of various chimera heads across a wide region of the parameter space. However, the CT value indicates that most of the heads rapidly collapse. Multiple heads emerge; however, they do not remain stable and transition to a synchronized state. The top panel in Fig. 3(b) shows that the number of heads decreases when the time is equal to 100. There is a range in the parameter space in which multi-headed chimeras persist until 100 s. Increasing to 500 s, the size of the yellow region decreases, leading to states in which the chimeras have one single head or disappear, as displayed in Fig. 3(c). According to the CT values, some chimeras with one head can persist for a long time. Depending on R and g_{syn}, it is possible to observe multi-head chimeras over time. The chimeras are predominantly

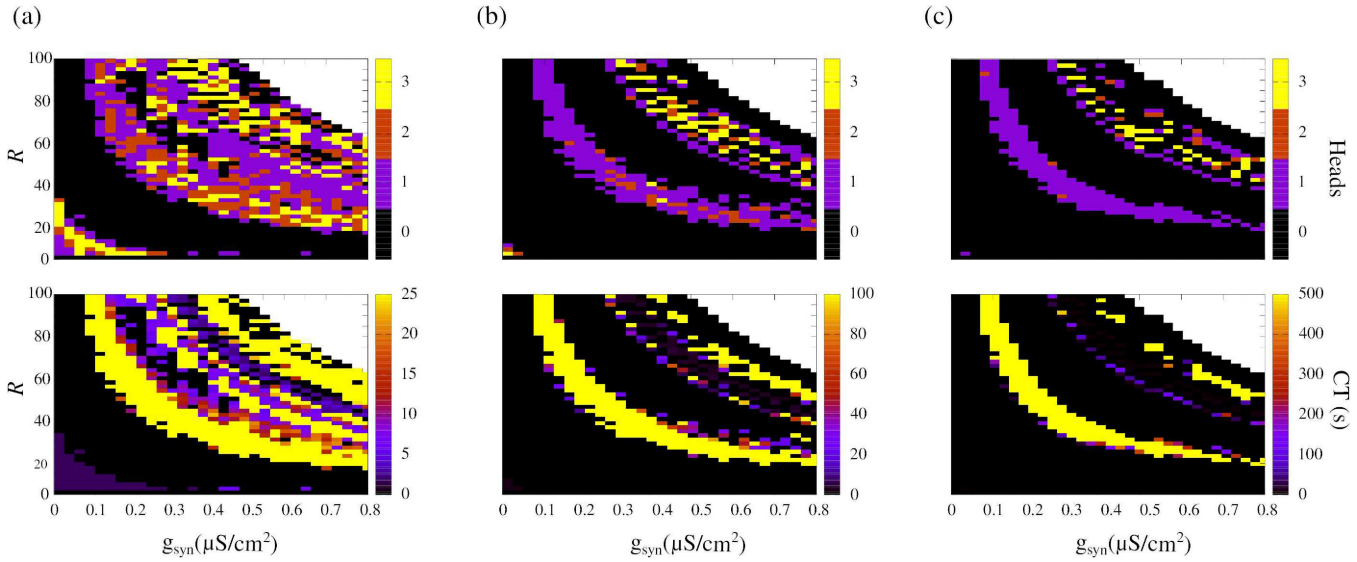


FIG. 3. $R \times g_{syn}$ showing the number of chimera heads (top panels) for (a) 25, (b) 100, and (c) 500 s, as well as the respective collapse times (bottom panels) from the time equal to 0.

22 September 2025 13:44:29

Published under an exclusive license by AIP Publishing

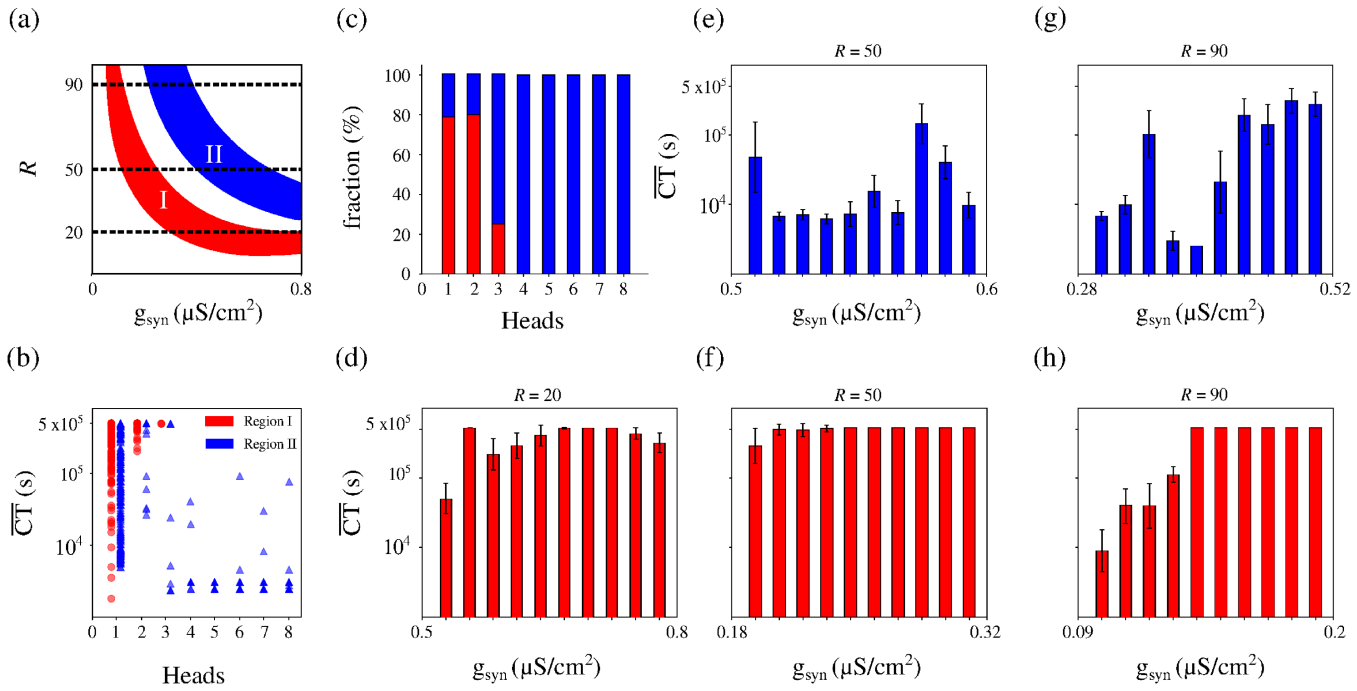


FIG. 4. (a) $R \times g_{syn}$ for the time equal to 500 s. In Region I (red) and Region II (blue), the fractions of initial conditions that converge to single- and multi-headed chimeras are greater, respectively. (b) CT vs the number of CHs for different initial conditions, where the red circles and blue triangles correspond to Region I and Region II. (c) Fraction of the number of heads in each colored region. The average value of CT as a function of g_{syn} for $R = 20$ in panel (d), $R = 50$ in panels (e) and (f), and $R = 90$ in panels (g) and (h) according to the black dashed lines in panel (a).

characterized by a single head, suggesting that they are more stable than multi-headed chimeras.

Aiming to investigate the dependence of the chimeras on the initial conditions, we separate the parameter space $R \times g_{syn}$ into Region I (red) and Region II (blue) for the time equal to 500 s, as displayed in Fig. 4(a). It is possible to identify chimera states in both regions. According to Fig. 4(b), in Region I, there are chimeras with one, two, and three heads that can persist for a very long time. Chimeras with more than three heads are found in Region II; however, they have short lifespans. In Fig. 4(c), we compute the fraction of the number of chimera heads. In Region I (II), we observe 78.4% (21.6%), 79.6% (20.4%), and 25% (75%) of chimeras with one, two, and three heads. The fractions of one, two, and three heads in Region I are greater than Region II. Chimeras with more than three heads are found only in Region II.

We compute the averaged value of CT (height) as a function of g_{syn} for $R = 20$ (low value), $R = 50$ (intermediate value), and $R = 90$ (high value), as displayed in panel (d), in panels (e) and (f), and in panels (g) and (h), respectively, according to the black dashed lines in Fig. 4(a). We performed 64 simulations per R with randomly generated initial conditions. The membrane potential V of each neuron is drawn from a normal distribution in the range $[-70, -50]$ mV, while the gating variables m, h, and n are initialized uniformly in $[0, 0.1]$. The remaining variables (p, q, r, and u) are fixed at zero. Each simulation was run for 500 s. The red and blue colors correspond to Regions I and II, respectively.

For $R = 20$, there is only Region I and the $\overline{CT}$ values are approximately greater than 5×10^4 with small error bars, as exhibited in Fig. 4(d). In Region I, for $R = 50$ [Fig. 4(f)] and $R = 90$ [Fig. 4(h)], the values of $\overline{CT}$ are high due to the fact that the chimeras take a long time to collapse. Figures 4(e) and 4(g) show that the values of $\overline{CT}$ are less than 5×10^5 in Region II. Therefore, the chimeras in Region II have collapse times shorter than those in Region I.

V. CONCLUSIONS

In this work, we investigate the dynamics of a locally coupled neuronal network composed of conductance-based excitatory neurons. By incorporating biologically realistic ionic currents, including sodium, potassium, and both high- and low-threshold calcium currents, we reproduce a variety of spatiotemporal patterns, including synchrony, asynchrony, bursting, and chimera states. Chimeras are characterized by the coexistence of coherent and incoherent activities within the same network.

The main focus of our study is the formation and collapse of chimera states. We demonstrate that the number of chimera heads depends on the network's nearest-neighbor connectivity R and synaptic conductance g_{syn}. With regard to these parameters, we show that multi-headed chimeras are more frequently observed in intermediate value ranges. In our results, we identify that multi-headed chimeras exhibit collapse times shorter than single-headed

22 September 2025 13:44:29

Published under an exclusive license by AIP Publishing

ones. Moreover, we explore how the initial conditions influence the collapse of chimeras.

By analyzing the parameter space $R \times g_{syn}$, we find a region in which there are chimeras with one, two, and three heads (Region I), as well as another region with chimeras exhibiting up to eight heads (Region II). We observe that the shorter collapse time in Region II is related to the higher number of connections and stronger synaptic coupling among the neurons. Consequently, the chimeras in Region II, particularly those with more than three heads, tend to collapse faster than those in Region I.

The novelty in our study is to combine a locally coupled network with conductance-based excitatory neurons to show the emergence of multi-headed chimera states. Overall, our findings highlight the interplay between connectivity, synaptic conductance, and initial conditions in the lifespan and structure of chimera states. Similar patterns of partial synchrony and collapse have been observed in brain dynamics, such as seizure initiation or breakdown of functional segregation. By using a biologically based model, our work provides a step toward connecting studies about chimeras patterns with more realistic neuronal models.

In future works, we plan to analyze the stability of multi-headed chimera states and how the mean collapse time depends on the number of heads. We will also investigate the collapse time for different network sizes.

ACKNOWLEDGMENTS

We would like to thank the following Brazilian government agencies: CNPq, CAPES (Finance Code 001; No. 88887.006227/2024-00-40006018; No. 88887.102678/2025-00), Fundação Araucária, and FAPESP (Nos. 2018/03211-6, 2022/13761-9, 2024/14478-4, and 2025/02318-5). R.L.V. received financial support from Conselho Nacional de Desenvolvimento Científico e Tecnológico (CNPq) under Grant Nos. 301019/2019-3, 403120/2021-7, 443575/2024-0, 446188/2024-7, and 315299/2025-8 and from Coordenação de Aperfeiçoamento de Pessoal de Nível Superior (CAPES) under Grant No. 88881.895032/2023-01. We thank 105 Group Science (www.105groupscience.com).

AUTHOR DECLARATIONS

Conflict of Interest

The authors have no conflicts to disclose.

Author Contributions

Lucas E. Bentivoglio: Conceptualization (equal); Data curation (equal); Formal analysis (equal); Investigation (equal); Methodology (equal); Validation (equal); Visualization (equal); Writing – original draft (equal); Writing – review & editing (equal). **Diogo L. M. Souza:** Conceptualization (equal); Investigation (equal); Validation (equal); Visualization (equal); Writing – review & editing (equal). **Enrique C. Gabrick:** Conceptualization (equal); Validation (equal); Visualization (equal); Writing – review & editing (equal). **Paulo R. Protachevicz:** Conceptualization (equal); Validation (equal); Visualization (equal); Writing – review & editing (equal). **Gustavo A. Sousa:** Conceptualization (equal); Validation (equal); Visualization (equal); Writing – review & editing (equal). **Iberê L. Caldas:** Conceptualization (equal); Funding acquisition (equal); Supervision (equal); Visualization (equal); Writing – review & editing (equal). **Ricardo L. Viana:** Conceptualization (equal); Funding acquisition (equal); Visualization (equal); Writing – review & editing (equal). **Kelly C. Iarosz:** Conceptualization (equal); Supervision (equal); Validation (equal); Visualization (equal); Writing – review & editing (equal). **Antonio M. Batista:** Conceptualization (equal); Funding acquisition (equal); Investigation (equal); Methodology (equal); Supervision (equal); Validation (equal); Visualization (equal); Writing – review & editing (equal). **Fernando S. Borges:** Conceptualization (equal); Data curation (equal); Funding acquisition (equal); Investigation (equal); Methodology (equal); Validation (equal); Visualization (equal); Writing – review & editing (equal).

DATA AVAILABILITY

The data that support the findings of this study are available from the corresponding author upon reasonable request.

REFERENCES

[1] K. T. Alligood, T. D. Sauer, and J. A. Yorke, *Chaos: An Introduction to Dynamical Systems* (Springer, New York, 1998).
[2] J. Gómez-Gardenes, Y. Moreno, and A. Arenas, "Paths to synchronization on complex networks," Phys. Rev. Lett. **98**, 034101 (2007).
[3] Q. Wang, Z. Duan, M. Perc, and G. Chen, "Synchronization transitions on small-world neuronal networks: Effects of information transmission delay and rewiring probability," Europhys. Lett. **83**, 50008 (2008).
[4] A. Pikovsky, M. Rosenblum, and J. Kurths, *Synchronization: A Universal Concept in Nonlinear Sciences* (Cambridge University Press, 2001).
[5] S. H. Strogatz and I. Stewart, "Coupled oscillators and biological synchronization," Europhys. Lett. **269**, 102–109 (1993).
[6] Y. Lei, X. J. Xu, X. Wang, Y. Zou, and J. Kurths, "A new criterion for optimizing synchrony of coupled oscillators," Chaos, Solitons Fractals **168**, 113192 (2023).
[7] D. M. Abrams and S. H. Strogatz, "Chimera states for coupled oscillators," Phys. Rev. Lett. **93**, 174102 (2004).
[8] V. Santos, F. S. Borges, K. C. Iarosz, I. L. Caldas, R. L. Viana, M. S. Baptista, and A. M. Batista, "Basin of attraction for chimera states in a network of Rössler oscillators," Chaos **30**, 063126 (2020).
[9] E. V. Rybalova, A. Zakharova, and G. I. Strelkova, "Interplay between solitary states and chimeras in multiplex neural networks," Chaos, Solitons Fractals **148**, 111011 (2021).
[10] Z. Wang, Y. Xu, Y. Li, T. Kapitaniak, and J. Kurths, "Chimera states in coupled Hindmarsh-Rose neurons with α-stable noise," Chaos, Solitons Fractals **148**, 110976 (2021).
[11] Y. Kuramoto and D. Battogtokh, "Coexistence of coherence and incoherence in nonlocally coupled phase oscillators," Nonlinear Phenom. Complex Syst. **5**, 380–385 (2002).
[12] M. R. Tinsley, S. Nkomo, and K. Showalter, "Chimera and phase-cluster states in populations of coupled chemical oscillators," Nat. Phys. **8**, 662–665 (2012).
[13] J. F. Totz, J. Rode, M. R. Tinsley, K. Showalter, and H. Engel, "Spiral wave chimera states in large populations of coupled chemical oscillators," Nat. Phys. **14**, 282–285 (2018).
[14] A. M. Hagerstrom, T. E. Murphy, R. Roy, P. Hövel, I. Omelchenko, and E. Schöll, "Experimental observation of chimeras in coupled-map lattices," Nat. Phys. **8**, 658–661 (2012).
[15] R. Sarfati and O. Peleg, "Chimera states among synchronous fireflies," Sci. Adv. **8**(46), eadd6690 (2022).
[16] C. Yang, M. S. Santos, P. R. Protachevicz, P. D. dos Reis, K. C. Iarosz, I. L. Caldas, and A. M. Batista, "Chimera states induced by spike timing-dependent plasticity in a regular neuronal network," AIP Adv. **12**(10), 105119 (2022).

22 September 2025 13:44:29

Published under an exclusive license by AIP Publishing

[17]X. Li, Y. Xie, Z. Ye, W. Huang, L. Yang, X. Zhan, and Y. Jia, "Chimera-like state in the bistable excitatory-inhibitory cortical neuronal network," Chaos, Solitons Fractals **180**, 114549 (2024).
[18]D. L. M. Souza, F. S. Borges, E. C. Gabrick, L. E. Bentivoglio, P. R. Protachevicz, V. dos Santos, R. L. Viana, I. L. Caldas, K. C. Iarosz, A. M. Batista, and J. Kurths, "Spiral wave dynamics in a neuronal network model," J. Phys. Complex. **5**(2), 025010 (2024).
[19]L. M. Mukhametov, A. Y. Supin, and I. G. Polyakova, "Interhemispheric asymmetry of the electroencephalographic sleep patterns in dolphins," Brain Res. **134**, 581–584 (1977).
[20]N. C. Rattenborg, C. J. Amlaner, and S. L. Lima, "Behavioral, neurophysiological and evolutionary perspectives on unihemispheric sleep," Neurosci. Biobehav. Rev. **24**(8), 817–842 (2000).
[21]E. Tognoli and J. A. S. Kelso, "The metastable brain," Neuron **81**(1), 35–48 (2014).
[22]M. S. Santos, P. R. Protachevicz, K. C. Iarosz, I. L. Caldas, R. L. Viana, F. S. Borges, H. P. Ren, J. D. Szezech, Jr., A. M. Batista, and C. Grebogi, "Spike-burst chimera states in an adaptive exponential integrate-and-fire neuronal network," Chaos **29**, 043106 (2019).
[23]F. S. Borges, E. C. Gabrick, P. R. Protachevicz, G. S. V. Higa, E. L. Lameu, P. X. R. Rodriguez, M. S. A. Ferraz, J. D. Szezech, Jr., A. M. Batista, and A. H. Kihara, "Intermittency properties in a temporal lobe epilepsy model," Epilepsy Behav. **139**, 109072 (2023).
[24]S. Majhi, B. K. Bera, D. Ghosh, and M. Perc, "Chimera states in neuronal networks: A review," Phys. Life Rev. **28**, 100–121 (2019).
[25]A. Provata and I. E. Venetis, "Chimera states in leaky integrate-and-fire dynamics with power law coupling," Eur. Phys. J. B **93**, 160 (2020).
[26]A. Calim, P. Hövel, M. Ozer, and M. Uzuntarla, "Chimera states in networks of type-I Morris-Lecar neurons," Phys. Rev. E **98**(6), 062217 (2018).
[27]I. Omelchenko, A. Provata, J. Hizanidis, E. Schöll, and P. Hövel, "Robustness of chimera states for coupled FitzHugh-Nagumo oscillators," Phys. Rev. E **91**(2), 022917 (2015).
[28]J. Hizanidis, N. E. Kouvaris, G. Zamora-López, A. Díaz-Guilera, and C. G. Antonopoulos, "Chimera-like states in modular neural networks," Sci. Rep. **6**(1), 19845 (2016).
[29]T. A. Glaze, S. Lewis, and S. Bahar, "Chimera states in a Hodgkin-Huxley model of thermally sensitive neurons," Chaos **26**(8), 083117 (2016).
[30]M. S. Santos, J. D. Szezech, F. S. Borges, K. C. Iarosz, I. L. Caldas, A. M. Batista, R. L. Viana, and J. Kurths, "Chimera-like states in a neuronal network model of the cat brain," Chaos, Solitons Fractals **101**, 86–91 (2017).
[31]J. M. Bekkers, "Pyramidal neurons," Curr. Biol. **21**(24), R975 (2011).
[32]P. Dayan and L. F. Abbott, *Theoretical Neuroscience: Computational and Mathematical Modeling of Neural Systems* (MIT Press, 2005).
[33]W. Gerstner, W. M. Kistler, R. Naud, and L. Paninski, *Neuronal Dynamics: From Single Neurons to Networks and Models of Cognition* (Cambridge University Press, 2014).
[34]A. L. Hodgkin and A. F. Huxley, "A quantitative description of membrane current and its application to conduction and excitation in nerve," J. Physiol. **117**(4), 500–544 (1952).
[35]W. M. Yamada, C. Koch, and P. R. Adams, "Multiple channels and calcium dynamics," in *Methods in Neuronal Modeling*, edited by C. Koch and I. Segev (MIT Press, 1989), pp. 137–170.
[36]I. Reuveni, A. Friedman, Y. Amitai, and M. J. Gutnick, "Stepwise repolarization from Ca^{2+} plateaus in neocortical pyramidal cells: Evidence for nonhomogeneous distribution of HVA Ca^{2+} channels in dendrites," J. Neurosci. **13**(11), 4609–4621 (1993).
[37]A. Destexhe, T. Bal, D. A. McCormick, and T. J. Sejnowski, "Ionic mechanisms underlying synchronized oscillations and propagating waves in a model of ferret thalamic slices," J. Neurophysiol. **76**(3), 2049–2070 (1996).
[38]R. D. Traub and R. Miles, *Neuronal Networks of the Hippocampus* (Cambridge University Press, 1991).
[39]F. S. Borges, P. R. Protachevicz, D. L. Souza, C. F. Bittencourt, E. C. Gabrick, L. E. Bentivoglio, J. D. Szezech, Jr., A. M. Batista, I. L. Caldas, S. Dura-Bernal, and R. F. Pena, "The roles of potassium and calcium currents in the bistable firing transition," Brain Sci. **13**(9), 1347 (2023).
[40]M. Pospischil, M. Toledo-Rodriguez, C. Monier, Z. Piwkowska, T. Bal, Y. Frégnac, H. Markram, and A. Destexhe, "Minimal Hodgkin-Huxley type models for different classes of cortical and thalamic neurons," Biol. Cybern. **99**, 427–441 (2008).
[41]J. R. Huguenard and D. A. McCormick, "Simulation of the currents involved in rhythmic oscillations in thalamic relay neurons," J. Neurophysiol. **68**(4), 1373–1383 (1992).
[42]Y. Kuramoto, *Chemical Turbulence* (Springer, Berlin, 1984), pp. 111–140.
[43]I. Omelchenko, O. E. Omel'chenko, P. Hövel, and E. Schöll, "When nonlocal coupling between oscillators becomes stronger: Patched synchrony or multichimera states," Phys. Rev. Lett. **110**(22), 224101 (2013).

22 September 2025 13:44:29

Published under an exclusive license by AIP Publishing